International Journal of Solids and Structures 51 (2014) 2706–2712

Contents lists available at ScienceDirect

International Journal of Solids and Structures

journal homepage: www.elsevier.com/locate/ijsolstr

Adhesion between elastic cylinders based on the double-Hertz model

Fan Jin [a,b], Wei Zhang [a], Sulin Zhang [c], Xu Guo [a,*]

[a] State Key Laboratory of Structural Analysis for Industrial Equipment, Department of Engineering Mechanics, Dalian University of Technology, Dalian 116023, PR China
[b] Institute of Systems Engineering, China Academy of Engineering Physics, Mianyang, Sichuan 621900, PR China
[c] Department of Engineering Science and Mechanics, Department of Materials Science and Engineering, The Pennsylvania State University, University Park, PA 16802, United States

ARTICLE INFO

Article history:
Received 10 November 2013
Received in revised form 29 March 2014
Available online 13 April 2014

Keywords:
Contact mechanics
Adhesion
Cohesive zone model
Double-Hertz model
Surface energy

ABSTRACT

A cohesive zone model for two-dimensional adhesive contact between elastic cylinders is developed by extending the double-Hertz model of Greenwood and Johnson (1998). In this model, the adhesive force within the cohesive zone is described by the difference between two Hertzian pressure distributions of different contact widths. Closed-form analytical solutions are obtained for the interfacial traction, deformation field and the equilibrium relation among applied load, contact half-width and the size of cohesive zone. Based on these results, a complete transition between the JKR and the Hertz type contact models is captured by defining a dimensionless transition parameter μ, which governs the range of applicability of different models. The proposed model and the corresponding analytical results can serve as an alternative cohesive zone solution to the two-dimensional adhesive cylindrical contact.

1. Introduction

Adhesive forces that act between contacting bodies play a key role in determining the mechanical behavior of small-scale systems. For instance, adhesive force can induce significant local stress in atomic force microscopy (AFM) which can therefore result in substantial wear and tip degradation (Liu et al., 2010). With increasing usage of micro-scale components and devices, it is imperative to obtain a better understanding of the contact behavior considering adhesive forces.

Since Hertz's seminal work (1882) on the unilateral contact of elastic spheres, numerous studies have been conducted on the adherence of spherical bodies. Bradley (1932) examined the attractive force between two rigid spheres by considering the molecular interactions. Later on, two famous models for adhesive contact between elastic spheres were proposed by Johnson et al. (1971) (JKR model) and Derjaguin et al. (1975) (DMT model), respectively. However, the magnitudes of the pull-off force predicted by the JKR and DMT models are quite different. Tabor (1977) then compared the two models and showed that JKR and DMT models represent two limiting cases of adhesive contact and their ranges of validity can be assessed by a dimensionless parameter (i.e., Tabor parameter) (Greenwood, 1997; Johnson and Greenwood, 1997; Barthel, 2008). To be more specific, the JKR model works well for soft materials with relatively high surface energy while the DMT model is more appropriate for hard solids with low surface energy. The first cohesive zone model which can allow for the transition between the JKR and DMT models was established by Maugis (1992). In this model (the so-called Maugis–Dugdale (M–D) model), the adhesive stress acting over the cohesive zone is assumed to be constant (i.e., Dugdale (1960)), which facilitates the derivation of analytical solutions. Soon afterwards, this model was also extended to describe the noncontact case (Kim et al., 1998).

In parallel with the M–D model, Greenwood and Johnson (1998) put forward an alternative cohesive zone model, known as the double-Hertz (D-H) model, which is also applicable to arbitrary values of Tabor parameter. In this model, the adhesive force within the cohesive zone is described by the difference between two Hertzian pressure distributions of different contact radii. It was found that results obtained by the D-H model are very close to those from the M–D model. However, the D-H model is more analytically tractable than the M–D model since the corresponding analysis relies solely on the classical Hertzian solutions. For this reason, the D-H model is often adopted to study the adhesion behavior of complex contact systems involving rough contact surfaces (Persson, 2002; Zhang et al., 2014), viscoelastic materials (Haiat et al., 2003) and functionally graded elastic solids (Jin et al., 2013). Recently, the D-H model was reconsidered in a slightly different context using an auxiliary function method (Barthel, 2012).

The above advances in contact mechanics of three-dimensional spherical bodies laid a solid foundation for the study of two-dimensional cylindrical contact systems. Barquins (1988) developed the

* Corresponding author. Tel.: +86 411 84707807.
E-mail address: guoxu@dlut.edu.cn (X. Guo).

http://dx.doi.org/10.1016/j.ijsolstr.2014.04.003
0020-7683/

JKR-type solutions for elastic cylinders and verified it experimentally. With use of Barquins's theory, Chaudhury et al. (1996) predicted the surface and adhesion energies of elastomeric polydimethylsiloxane (PDMS) successfully. The two-dimensional JKR model was also extended to the non-slipping case with the frictionless contact assumption relaxed (Chen and Gao, 2006a; 2007) and the conforming contact case with the half-plane assumption relaxed (Sundaram et al., 2012).

The above mentioned JKR-based models, however, do not consider the adhesion forces outside the contact area and therefore are only applicable to soft bodies with relatively large Tabor parameters. For general material properties, Baney and Hui (1997) proposed the first cohesive zone model for cylindrical contact in the framework of M–D model, Morrow and Lovell (2005) then extended Baney and Hui's theory to the case where the surfaces are not within intimate contact but are within the range of adhesive interaction. The same two-dimensional M–D analysis was also performed by Johnson and Greenwood (2008) independently, with emphasis on the pull-off force. Chen and Gao (2006b) presented an analogous M-D model of a cylinder in non-slipping adhesive contact with a stretched substrate. Furthermore, based on the two-dimensional M-D model, Sari et al. (2005) also investigated the sliding and rolling motion of a cylinder on the substrate subjected to combined normal and tangential forces.

The present study is aimed to extend the three-dimensional double-Hertz model of Greenwood and Johnson (1998) to a plane strain problem, with emphasis on establishing a set of simple analytical solutions which are applicable for a full range of Tabor parameters. These solutions can not only describe a complete transition between the two-dimensional JKR and the Hertz type contact models, but also exhibit as equally effective as the two-dimensional M–D model.

The rest of the paper is organized as follows. We first extend the double-Hertz model to the cylindrical contact system in Section 2. The main analytical results are then presented in dimensionless form in Section 3. Section 4 discusses the reduction of the proposed model in two limiting cases of small and large cohesive zones. The traction-separation relation within the cohesive zone is examined in Section 5. Finally, some concluding remarks are provided in Section 6.

2. Two-dimensional double-Hertz model

Fig. 1a shows the adhesive contact between two dissimilar elastic cylinders with parallel axes under a prescribed load P (with unit N/m and negative when tensile). Contact occurs over a rectangular region of width $2a$. In fact, if the tangential tractions are neglected, this problem is equivalent to the plain strain frictionless contact problem between a rigid cylinder of radius R and an elastic half-plane with a effective Young's modulus E^*, where

$$1/R = 1/R_1 + 1/R_2 \tag{2.1}$$

and

$$1/E^* = (1-\nu_1^2)/E_1 + (1-\nu_2^2)/E_2, \tag{2.2}$$

respectively. In Eqs. (2.1) and (2.2), R_1, R_2 are the radii, ν_1, ν_2 are the Poisson radios and E_1, E_2 are the Young's moduli of the contacting cylinders, respectively (Johnson, 1985). For subsequent analytical treatment, as shown in Fig. 1b, a Cartesian coordinate system (x, z) is set up with origin at the center of the contact zone and z direction pointing into the half-plane. The distribution of surface traction consists of two terms: the Hertz pressure p_H acting on a contact region of width $2a$ and the adhesive tension p_A acting on an interaction zone of width $2c$. The noncontact regions bounded by half-widths a and c (i.e., $a \leqslant |x| \leqslant c, z = 0$) are known as the cohesive

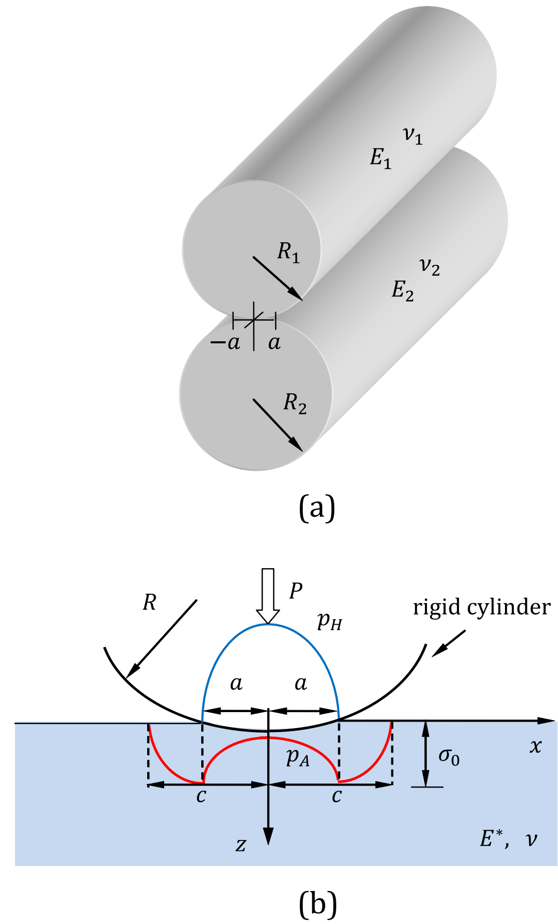

Fig. 1. (a) Schematics of adhesive contact between two elastic cylinders. The constants (E_1, ν_1) and (E_2, ν_2) denote Young's moduli and Poisson's ratios of the two cylinders. (b) A rigid cylinder in frictionless adhesive contact with an elastic half-plane under a normal load P (negative when tensile). The distribution of surface traction consists of two terms: the Hertz pressure p_H acting on the contact zone of width $2a$ and an adhesive traction p_A acting on the interaction zone of width $2c$.

zones. Since the present problem is symmetry with respect to the z-axis, we only quote the equations for $x \geqslant 0$ in the following analysis.

In the absence of adhesive force, the Hertz-type pressure distribution between a rigid cylinder and an elastic half-plane is given by (Johnson, 1985)

$$p(x) = \frac{E^*}{2R}(a^2 - x^2)^{1/2}, \quad |x| \leqslant a \tag{2.3}$$

which corresponds to a prescribed load

$$P = \frac{\pi a^2 E^*}{4R} \tag{2.4}$$

The derivative of the surface normal displacement with respect to x can be expressed as

$$\frac{\partial u_z}{\partial x} = -\frac{x}{R}, \quad 0 \leqslant x \leqslant a, \tag{2.5a}$$

$$\frac{\partial u_z}{\partial x} = -\frac{2}{\pi E^*}\int_{-a}^{a}\frac{p(s)}{x-s}\mathrm{d}s = -\frac{x-\sqrt{x^2-a^2}}{R}, \quad x \geqslant a, \tag{2.5b}$$

According to Greenwood and Johnson (1998), the essential idea behind the proposed two-dimensional double-Hertz model is to represent the adhesive tensile traction by resorting to the difference of two Hertzian pressure distributions, that is,

$$p(x) = \frac{E^*}{2R}\left[(c^2 - x^2)^{1/2} - (a^2 - x^2)^{1/2}\right], \quad 0 \leqslant x \leqslant a, \tag{2.6a}$$

$$p(x) = \frac{E^*}{2R}(c^2 - x^2)^{1/2}, \quad a \leqslant x \leqslant c. \tag{2.6b}$$

Furthermore, we also have

$$\frac{\partial u_z}{\partial x} = 0, \quad 0 \leqslant x \leqslant a \tag{2.7a}$$

and

$$\frac{\partial u_z}{\partial x} = -\frac{x}{R} + \frac{x - \sqrt{x^2 - a^2}}{R} = -\frac{\sqrt{x^2 - a^2}}{R}, \quad a \leqslant x \leqslant c, \tag{2.7b}$$

respectively.

Denoting $p_0 = aE^*/2R$, Fig. 2 plots the distributions of the normalized pressures p/p_0 resulting from the difference between two Hertzian solutions with contact half-widths a and c as shown in Eq. (2.6). It can be observed from this figure that the ellipsoidal pressure distribution over $a \leqslant |x| \leqslant c$ steadily decreases from the maximum value at $x = a$ to zero at $x = c$. In the following, the pressure in Eq. (2.6b) scaled by an arbitrary factor $\lambda(>0)$ will be employed to model the adhesive tensile traction over $a \leqslant |x| \leqslant c$, resulting in the final distribution of surface traction when combined with an original unscaled Hertzian pressure. Under this treatment, the interfacial traction for $0 \leqslant x \leqslant c$ can be written as

$$p_A(x) = -\frac{\lambda E^*}{2R}\left[(c^2 - x^2)^{1/2} - (a^2 - x^2)^{1/2}\right], \quad 0 \leqslant x \leqslant a, \tag{2.8a}$$

$$p_A(x) = -\frac{\lambda E^*}{2R}(c^2 - x^2)^{1/2}, \quad a \leqslant x \leqslant c. \tag{2.8b}$$

Denoting the maximum magnitude of interfacial traction as

$$\sigma_0 = \frac{\lambda E^*}{2R}(c^2 - a^2)^{1/2}, \tag{2.9}$$

which can be chosen, somewhat arbitrarily, to match that of the Lennard–Jones potential. Eq. (2.8) can be re-written in terms of σ_0 as

$$p_A(x) = -\frac{\sigma_0}{(c^2 - a^2)^{1/2}}\left[(c^2 - x^2)^{1/2} - (a^2 - x^2)^{1/2}\right], \quad 0 \leqslant x \leqslant a, \tag{2.10a}$$

$$p_A(x) = -\frac{\sigma_0}{(c^2 - a^2)^{1/2}}(c^2 - x^2)^{1/2}, \quad a \leqslant x \leqslant c. \tag{2.10b}$$

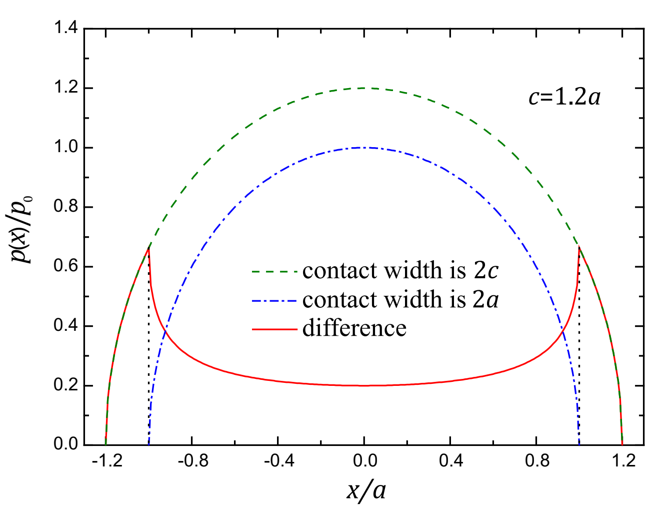

Fig. 2. The difference between two Hertzian solutions with contact half-widths a and c for surface pressure. Here, $p_0 = aE^*/2R$.

which corresponds to an applied load

$$P = \frac{\pi E^*}{4R}\left[a^2 - \lambda(c^2 - a^2)\right]. \tag{2.11}$$

Within the cohesive zone $a \leqslant x \leqslant c$, the derivative of the surface normal displacement is given by

$$\frac{\partial u_z}{\partial x} = \frac{(1+\lambda)\sqrt{x^2 - a^2}}{R} - \frac{x}{R} \tag{2.12}$$

and the resulting separation between the rigid cylinder and the deformed half-plane surface is obtained from the geometric relation as

$$h = -\delta + \frac{x^2}{2R} + u_z, \tag{2.13}$$

and accordingly

$$\frac{\mathrm{d}h}{\mathrm{d}x} = \frac{1+\lambda}{R}\sqrt{x^2 - a^2}, \quad a \leqslant x \leqslant c. \tag{2.14}$$

In Eq. (2.13), δ denotes the indentation depth at contact center. Recalling the fact that $h(a) = 0$, the separation can be derived from Eq. (2.14) as

$$h(x) = \frac{1+\lambda}{2R}\left[x\sqrt{x^2 - a^2} - a^2 \ln\left(\frac{x + \sqrt{x^2 - a^2}}{a}\right)\right], \quad a \leqslant x \leqslant c. \tag{2.15}$$

The surface energy is defined as the work needed to separate two surfaces to infinity. Since the separation vanishes for $0 \leqslant x \leqslant a$ and the traction vanishes for $x \geqslant c$, we have

$$\begin{aligned}\Delta\gamma &= -\int_0^\infty p_A(h)\mathrm{d}h = -\int_a^c p_A(x)\frac{\mathrm{d}h}{\mathrm{d}x}\mathrm{d}x \\ &= \frac{\lambda(1+\lambda)E^*}{2R^2}\int_a^c \sqrt{(x^2 - a^2)(c^2 - x^2)}\mathrm{d}x \\ &= \frac{\lambda(1+\lambda)E^*}{6R^2}\left[c(c^2 + a^2)E\left(\frac{\sqrt{c^2 - a^2}}{c}\right) - 2ca^2 K\left(\frac{\sqrt{c^2 - a^2}}{c}\right)\right],\end{aligned} \tag{2.16}$$

where $K(\cdot)$ and $E(\cdot)$ are the complete elliptic integral of the first and second kinds, respectively.

To determine λ, a transition parameter is introduced as (Baney and Hui, 1997)

$$\mu = \frac{4}{\pi^{2/3}}\mu_T = 4\left(\frac{R\Delta\gamma^2}{\pi^2 E^{*2} z_0^3}\right)^{1/3} \approx 4\sigma_0\left(\frac{R}{\pi^2 E^{*2}\Delta\gamma}\right)^{1/3}, \tag{2.17}$$

where μ_T denotes the classical Tabor parameter, which represents the ratio of the elastic displacement of the surfaces at pull-off to the effective range of surface forces characterized by z_0 (Tabor, 1977). Under this condition, a relationship between λ and μ can be established by combining Eqs. (2.9) and (2.17) as follows

$$\mu = 2\lambda(c^2 - a^2)^{1/2}\left(\frac{E^*}{\pi^2 R^2 \Delta\gamma}\right)^{1/3}. \tag{2.18}$$

Up to this point, main equilibrium equations of the two-dimensional double-Hertz model have been established.

3. Nondimensional results

In this section, the above results are summarized in a dimensionless form. By introducing the following nondimensional parameters:

$$a^* = \frac{a}{\eta}, \quad c^* = \frac{c}{\eta}, \quad m = \frac{c}{a}, \quad P^* = \frac{P}{(\pi R E^* \Delta\gamma^2)^{1/3}} \tag{3.1}$$

with

$$\eta = 2\left(\frac{R^2\Delta\gamma}{\pi E^*}\right)^{1/3}, \tag{3.2}$$

the dimensionless normal load can be obtained from Eq. (2.11) as

$$P^* = a^{*2} - \lambda(c^{*2} - a^{*2}), \tag{3.3}$$

and the relationship between a and c defined in Eq. (2.16) can be normalized as

$$1 = \frac{4\lambda(1+\lambda)}{3\pi}\left[c^*(c^{*2}+a^{*2})E\left(\frac{\sqrt{c^{*2}-a^{*2}}}{c^*}\right) - 2c^*a^{*2}K\left(\frac{\sqrt{c^{*2}-a^{*2}}}{c^*}\right)\right], \tag{3.4}$$

where λ is related to the transition parameter through

$$\mu = \frac{4\lambda}{\pi}(c^{*2} - a^{*2})^{1/2}. \tag{3.5}$$

By eliminating λ, the $c \sim a$ relation can also be established in an implicit form as

$$3(c^{*2}-a^{*2}) = \mu\left[\sqrt{c^{*2}-a^{*2}} + \frac{\pi}{4}\mu\right] \times \left[c^*(c^{*2}+a^{*2})E\left(\frac{\sqrt{c^{*2}-a^{*2}}}{c^*}\right) - 2c^*a^{*2}K\left(\frac{\sqrt{c^{*2}-a^{*2}}}{c^*}\right)\right]. \tag{3.6}$$

Eqs. (3.3)–(3.5) can be compared to the two-dimensional Hertzian (Johnson, 1985), JKR (Barquins, 1988) and Maugis–Dugdale (Baney and Hui, 1997; Johnson and Greenwood, 2008) results, which are

$$P^*_{\mathrm{Hertz}} = a^{*2}, \quad P^*_{\mathrm{JKR}} = a^{*^2} - 2\sqrt{a^*} \tag{3.7a, b}$$

and

$$P^*_{\mathrm{M-D}} = a^{*2} - \mu a^*\sqrt{m^2-1} \tag{3.7c}$$

with

$$1 = \frac{\mu}{2}a^{*2}\left[m\sqrt{m^2-1} - \ln(m+\sqrt{m^2-1})\right] + \frac{\mu^2}{2}a^*\left[\sqrt{m^2-1}\ln(m+\sqrt{m^2-1}) - m\ln m\right]. \tag{3.7d}$$

Fig. 3 displays the equilibrium P–a curves in the present double-Hertz (D-H) model under various values of μ according to Eqs. (3.3)–(3.5). The corresponding Hertz, JKR and M–D solutions are also included for comparison. It can be seen that the D-H curves nearly coincide with the M–D solution and they approach the Hertz solution as μ is reduced to zero (e.g., $\mu = 0.01$). This is different from the adhesion problem of spheres, where the DMT solution is recovered for $\mu \to 0$. For moderate values of μ (e.g., $\mu = 4$), some deviation from the JKR solution remains noticeable especially for small contact sizes. For sufficiently large μ (e.g., $\mu = 10$), the JKR curve is readily approached. In fact, the JKR curve is expected to be fully recovered in the limit of $\mu \to \infty$, which will be discussed in detail in the next section.

Fig. 4 plots the half-widths of contact and interaction zones versus the applied load for various values of μ. From this figure, for larger μ the contact size a and the interaction zone size c are nearly the same, whilst for lower μ, c is far more than a. As the cohesive zone size is bounded by a and c, higher μ corresponds to a smaller cohesive zone whereas lower μ results in a larger cohesive zone.

In addition, the interfacial traction can be normalized as

$$p^*(x^*) = \begin{cases} a^*\sqrt{1-x^{*2}} - \frac{\pi\mu}{4\sqrt{m^2-1}}\left(\sqrt{m^2-x^{*2}} - \sqrt{1-x^{*2}}\right), & |x^*| \leqslant 1 \\ -\frac{\pi\mu\sqrt{m^2-x^{*2}}}{4\sqrt{m^2-1}}, & 1 \leqslant |x^*| \leqslant m \end{cases} \tag{3.8}$$

where

$$p^* = \frac{p}{\xi}, \quad x^* = \frac{x}{a}, \quad \xi = \left(\frac{E^{*2}\Delta\gamma}{\pi R}\right)^{1/3}. \tag{3.9}$$

The interfacial traction distributions for different values of μ for the case of $P^* = 1$ are illustrated in Fig. 5. It can be observed that the interfacial traction varies from a compressive value at contact center, through a maximum tensile value at contact edge, to zero at interaction fringe.

For comparison, Fig. 6 plots the D-H interfacial traction distributions for $P^* = 1$ and $\mu = 4$, along with the corresponding Hertz, JKR and M–D curves according to

$$p^*_{\mathrm{Hertz}}(x^*) = a^*\sqrt{1-x^{*2}},$$
$$p^*_{\mathrm{JKR}}(x^*) = a^*\sqrt{1-x^{*2}} - a^{*-\frac{1}{2}}(1-x^{*2})^{-\frac{1}{2}}, \quad |x^*| \leqslant 1, \tag{3.10a, b}$$

and

$$p^*_{\mathrm{MD}}(x^*) = \begin{cases} a^*\sqrt{1-x^{*2}} - \frac{\mu}{4}\arctan\sqrt{\frac{m^2-1}{1-x^{*2}}}, & |x^*| \leqslant 1 \\ -\frac{\pi\mu}{4}, & 1 \leqslant |x^*| \leqslant m. \end{cases} \tag{3.10c}$$

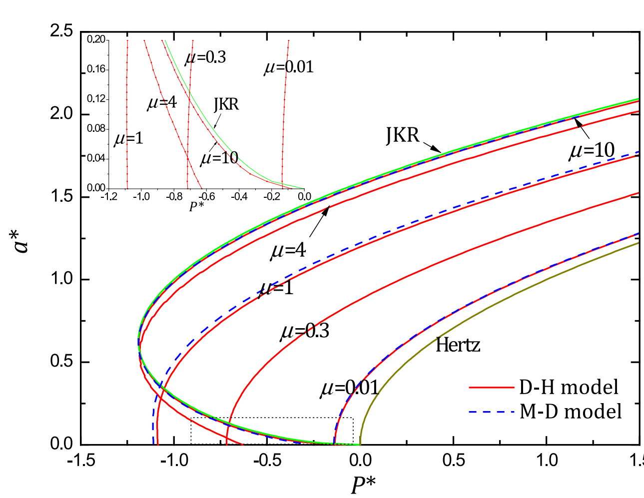

Fig. 3. The equilibrium P–a curves for various values of μ. The corresponding JKR, Hertzian and M–D solutions are also included for comparison.

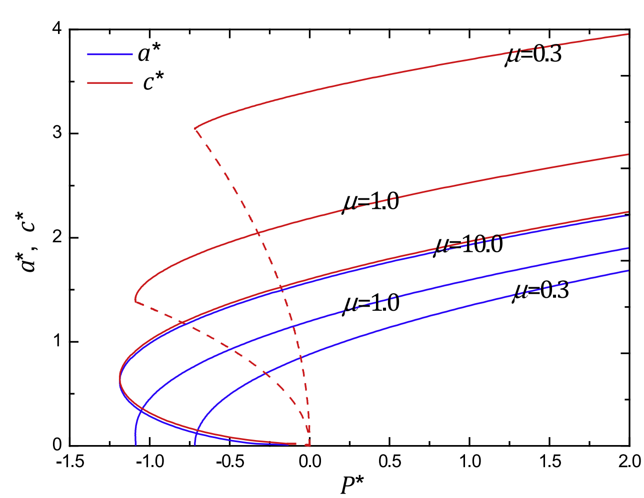

Fig. 4. The half-widths of contact and interaction zones versus the applied load for various values of μ. The dashed curves are the continuations for $a = 0$.

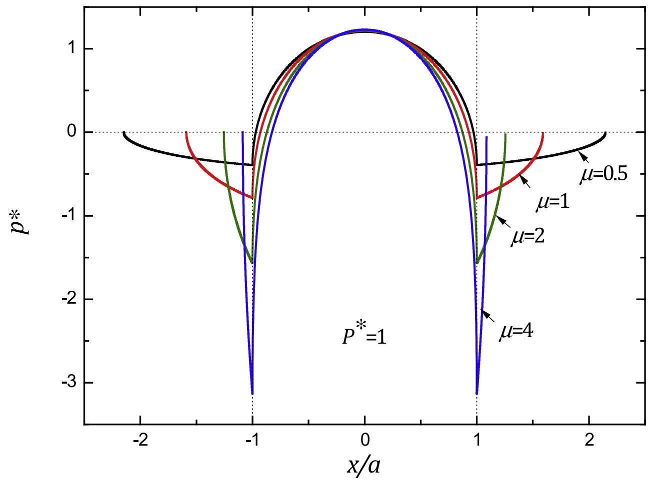

Fig. 5. Distributions of interfacial traction for various values of μ for $P^* = 1$.

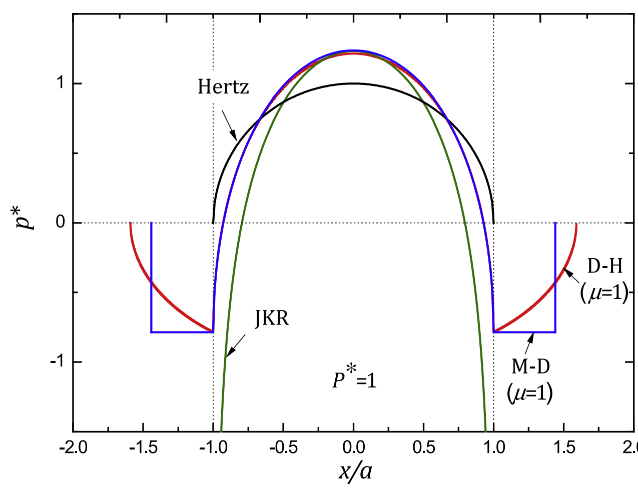

Fig. 6. Comparison of the distributions of interfacial traction predicted by the D-H model and the M–D model for $\mu = 1$ and $P^* = 1$ with the same σ_0 and $\Delta\gamma$.

It is noted that the maximum tensile traction $\sigma_0 = \pi\mu/4$ is predicted in both the D-H and M–D models. With the same σ_0 and $\Delta\gamma$, the interfacial tractions within the contact region, as shown in Fig. 6, are almost the same in the D-H and M–D models in spite of different adhesive traction forms within the cohesive zone.

4. Reduction

According to the classical cohesive zone models (Maugis, 1992; Greenwood and Johnson, 1998), a small cohesive zone applies to relatively large and soft bodies corresponding to a large Tabor parameter, while a large cohesive zone holds for small and rigid solids with a small Tabor number. This also holds true for the cylindrical contact case. In fact, the transition parameter μ (similar to the Tabor number) defined in Eq. (2.17) is related to the cohesive zone size. As found in Fig. 4, larger μ tends to reduce the cohesive zone size, whereas smaller μ corresponds to a large cohesive zone. To illustrate this point, we shall examine the equilibrium P–a curves in two special cases: small and large cohesive zones, respectively.

4.1. Small cohesive zone

As the cohesive zone becomes very small ($c \to a$), i.e.,

$$m - 1 = \varepsilon \ll 1, \tag{4.1}$$

the applied load in Eq. (3.3) and the $c \sim a$ relation in Eq. (3.6) become

$$P^* \cong a^{*2} - \frac{\mu\pi a^*}{4}\sqrt{2\varepsilon}, \tag{4.2}$$

$$1 \cong \frac{\pi\mu^2 a^*}{24\varepsilon}\left[(2+2\varepsilon+\varepsilon^2)E\left(\frac{\sqrt{2\varepsilon+\varepsilon^2}}{1+\varepsilon}\right) - 2K\left(\frac{\sqrt{2\varepsilon+\varepsilon^2}}{1+\varepsilon}\right)\right], \tag{4.3}$$

respectively.

Recalling the following asymptotic expansions for $|z| < 1$:

$$K(z) = \frac{\pi}{2}\left[1 + \left(\frac{1}{2}\right)^2 z^2 + \left(\frac{1.3}{2.4}\right)^2 z^4 + \cdots + \left(\frac{(2n-1)!!}{(2n)!!}\right)^2 z^{2n} + \cdots\right], \tag{4.4a}$$

$$E(z) = \frac{\pi}{2}\left[1 - \left(\frac{1}{2}\right)^2 \frac{z^2}{1} - \left(\frac{1.3}{2.4}\right)^2 \frac{z^4}{3} - \cdots - \left(\frac{(2n-1)!!}{(2n)!!}\right)^2 \frac{z^{2n}}{2n-1} - \cdots\right], \tag{4.4b}$$

Eq. (4.3) reduces to

$$\varepsilon \cong \frac{32}{\pi^2\mu^2 a^*}. \tag{4.5}$$

Inserting Eq. (4.5) back into Eq. (4.2) yields

$$P^* \cong a^{*2} - 2\sqrt{a^*}, \tag{4.6}$$

which is precisely the two-dimensional JKR result (Barquins, 1988). Note that Eq. (4.5) implies an additional condition on the contact half-width a as the JKR limit is recovered, i.e.,

$$\varepsilon \cong \frac{32}{\pi^2\mu^2 a^*} = \frac{4E^*\Delta\gamma}{\pi\sigma_0^2 a} \ll 1. \tag{4.7}$$

It is clear that the condition in Eq. (4.7) is generally valid as $\mu \to \infty$, and hence the JKR result can be viewed as the limit case of the present double-Hertz model for $\mu \to \infty$. For any finite value of μ, however, too small a^* cannot ensure Eq. (4.7) to be satisfied. This accounts for the noticeable deviation from the JKR curve at small a^* for moderate value of μ ($\mu = 4$), as shown in Fig. 3.

4.2. Large cohesive zone

When the cohesive zone is large compared to the contact zone, i.e., m $\gg 1$, the applied load in Eq. (3.3) and the $c \sim a$ relation in Eq. (3.6) are reduced to

$$P^* \cong a^{*2} - \frac{\pi\mu}{4}c^*, \tag{4.8}$$

$$1 \cong \frac{\mu}{3}c^*\left(c^* + \frac{\pi}{4}\mu\right). \tag{4.9}$$

Combining Eqs. (4.8) and (4.9) yields

$$c^* = -\frac{\pi\mu}{8}\left(1 - \sqrt{1 + \frac{192}{\pi^2\mu^3}}\right). \tag{4.10}$$

$$P^* \cong a^{*2} + \frac{\pi^2\mu^2}{32}\left(1 - \sqrt{1 + \frac{192}{\pi^2\mu^3}}\right). \tag{4.11}$$

For $\mu \ll 1$, Eq. (4.10) is reduced to

$$c^* \cong \sqrt{3/\mu}, \tag{4.12}$$

and accordingly

$$P^* \cong a^{*2}, \tag{4.13}$$

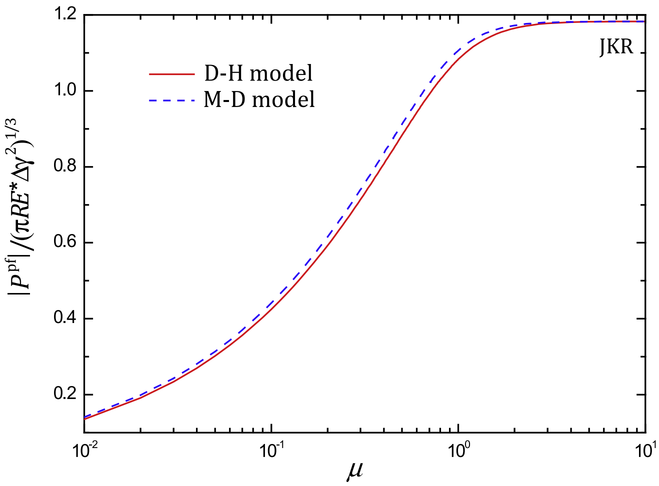

Fig. 7. Pull-off forces for cylindrical contacts as a function of the transition parameter predicted by the D-H model and the M–D model.

which coincides perfectly with the two-dimensional Hertzian solution (Johnson, 1985). Since there is no restriction on a^* in the present case, the Hertzian solution is approached for all values of a^* when $\mu \to 0$. This is quite different from that in the three dimensional (3-D) case where the DMT solution is approached as $\mu \to 0$. As pointed out by Baney and Hui (1997), the difference between 2-D and 3-D cases exists in the different ways that the adhesion forces scale with the characteristic contact size. This also holds true for the present double-Hertz model.

The variation of the pull-off force as a function of the transition parameter is shown in Fig. 7, together with the corresponding M–D curve. It can be seen that the magnitude of the pull-off forces predicted by these two cohesive zone models increase smoothly from zero for small μ to the JKR value for large μ. The JKR value can be calculated from Eq. (4.6) as $P^*_{\mathrm{JKR}} = -3/\sqrt[3]{16} \approx -1.19$, while the zero pull-off force has been demonstrated in Eq. (4.13). As a consequence, the Hertz and JKR models for cylindrical contacts are unified in the present double-Hertz model.

Fig. 8 shows the critical half-widths of contact and interaction zones at pull-off versus the transition parameter predicted by the D-H model and the M–D model. It can be observed that both decreasing c and increasing a approach to the JKR limit as μ grows to 10. Hence, JKR model can provide an accurate solution for adhesion of elastic cylinders with $\mu \geqslant 10$.

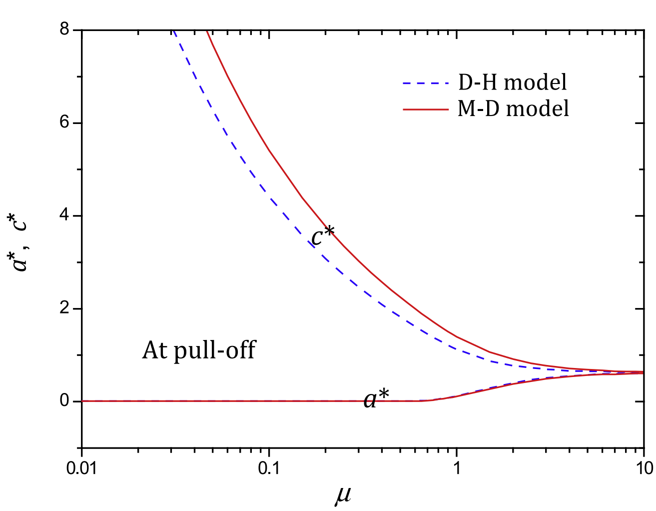

Fig. 8. The critical half-widths of contact and interaction zones at pull-off versus the transition parameter predicted by the D-H model and the M–D model.

5. Traction-separation relation

For various ratios of the interaction zone size c to contact zone size a, the dependence of the adhesive traction on the surface separation within the cohesive zone is implicitly determined by combining Eqs. (2.10b) and (2.15). In fact, it is confined between two asymptotic limits: small cohesive zone and noncontact cohesive zone.

5.1. Small cohesive zone

As the cohesive zone becomes very small ($c \to a$), the surface separation given by Eq. (2.15) is reduced to

$$h(x) \cong h_c \left(\frac{x^2 - a^2}{c^2 - a^2}\right)^{\frac{3}{2}}, \quad a \leqslant x \leqslant c. \tag{5.1}$$

where

$$h_c = \frac{1+\lambda}{12Ra}(c^2 - a^2)^{\frac{3}{2}}. \tag{5.2}$$

Recalling the adhesive traction given in Eq. (2.10b), the traction-separation relation can be obtained as

$$\frac{p_A}{\sigma_0} = -\left[1 - \left(\frac{h}{h_c}\right)^{2/3}\right]^{1/2}. \tag{5.3}$$

Accordingly, the surface energy is

$$\Delta\gamma = -\int_0^{h_c} p_A \mathrm{d}h = \frac{3\pi}{16}\sigma_0 h_c. \tag{5.4}$$

In contrast, the corresponding relation in the M–D model is

$$\Delta\gamma = \sigma_0 h_M, \tag{5.5}$$

where h_M is the corresponding separation at $x = \pm c$ and σ_0 is a uniform adhesive stress acting over the entire cohesive zone.

5.2. Noncontact cohesive zone

At the instant of detachment, the contact half-width shrinks to zero ($a = 0$) for the first time, the adhesive traction, the surface separation and the surface energy behave as

$$p_A(x) = -\sigma_0\left(1 - \frac{x^2}{c^2}\right)^{1/2}, \quad 0 \leqslant x \leqslant c, \tag{5.6}$$

$$h(x) = h(c)\frac{x^2}{c^2}, \quad 0 \leqslant x \leqslant c, \tag{5.7}$$

$$\Delta\gamma = \lambda(1+\lambda)\frac{E^* c^3}{6R^2}, \tag{5.8}$$

respectively, where

$$\sigma_0 = \frac{\lambda E^*}{2R}c, \quad h(c) = \frac{1+\lambda}{2R}c^2 = \frac{3}{2}\frac{\Delta\gamma}{\sigma_0}. \tag{5.9}$$

As a result, the traction-separation relation can be expressed as

$$\frac{p_A}{\sigma_0} = -\left(1 - \frac{h}{h(c)}\right)^{1/2}. \tag{5.10}$$

To investigate the dependence of the adhesive traction on the surface separation within the cohesive zone, Fig. 9 plots the variations in the traction-separation relation with different cohesive zone sizes ($c = 1.2a$ and $c = 3a$). In this figure the surface separation is normalized by h_c defined in Eq. (5.4). The Lennard–Jones and the M–D traction-separation laws are also shown for comparison. As approximations of the more realistic Lennard–Jones law, the D-H

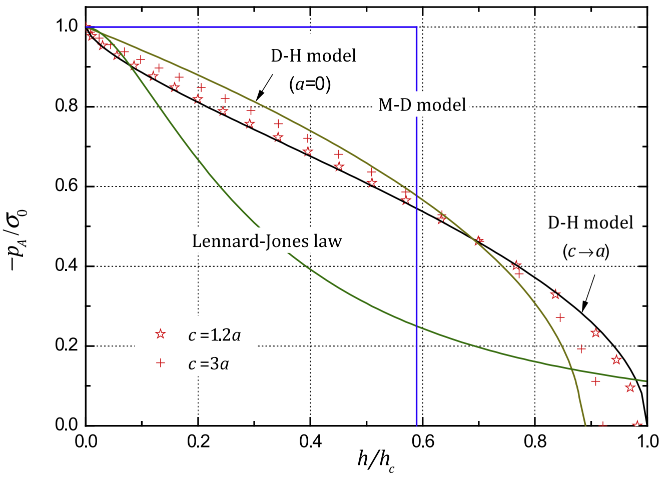

Fig. 9. Variations of the traction-separation relation with different cohesive zone sizes: $c = 1.2a$ (star) and $c = 3a$ (+). The Lennard–Jones law and the M–D force law with the same σ_0 and $\Delta\gamma$ are also shown for comparison. Here, h_c is defined in Eq. (5.4).

model and the M–D model have adopted different traction-separation relations and can be compared to each other under the same maximum traction σ_0 and work of adhesion $\Delta\gamma$. It is worth noting that the traction-separation relation in the double-Hertz model depends on the value of c/a but is strictly confined between two asymptotic limits (i.e., $c \to a$ and $a = 0$, respectively), which are given by Eqs. (5.3) and (5.10), respectively.

6. Conclusion

The present paper provides an alternative cohesive zone solution for 2-D adhesive cylindrical contact by extending the double-Hertz model of Greenwood and Johnson. This is achieved by describing the adhesive force in terms of the difference between two Hertzian pressures corresponding to different contact widths. Closed-form analytical solutions are obtained for the interfacial traction, deformation field and the equilibrium relation among applied load, contact half-width and the size of cohesive zone. Based on these results, a complete transition between the JKR and the Hertz type contact models is captured by defining a dimensionless transition parameter μ, which governs the range of applicability of different models. JKR and Hertz type solutions are included as two limiting cases of the present model. An interesting finding is that unlike the 3-D case, the Hertz type solution instead of DMT type solution is recovered for the case of small μ. In fact, this was also found in the M-D solution (Baney and Hui, 1997; Johnson and Greenwood, 2008), which is due to the fact that that the adhesion forces scale with the characteristic contact size in a quite different way under the 2-D and 3-D cases, respectively. The present work laid a foundation for investigating other complex adhesive cylindrical contact problems involving rough surfaces, viscoelastic materials and non-homogeneous materials. Corresponding results will be reported elsewhere.

Acknowledgements

The financial supports from the National Natural Science Foundation (10925209 and 91216201), 973 Project of China (2010CB832703), Program for Changjiang Scholars, Innovative Research Team in University (PCSIRT) and 111 Project (B14013) are gratefully acknowledged.

References

Baney, J.M., Hui, C.Y., 1997. A cohesive zone model for the adhesion of cylinders. J. Adhes. Sci. Technol. 11, 393–406.
Barquins, M., 1988. Adherence and rolling kinetics of a rigid cylinder in contact with a natural rubber surface. J. Adhes. 26, 1–12.
Barthel, E., 2008. Adhesive elastic contacts-JKR and more. J. Phys. D: Appl. Phys. 41, 163001.
Barthel, E., 2012. Adhesive contact: a few comments on cohesive zone models and self-consistency. J. Adhes. 88, 55–69.
Bradley, R.S., 1932. The cohesive force between solid surface and the surface energy of solids. Philos. Mag. 13, 853–862.
Chaudhury, M.K., Weaver, T., Hui, C.Y., Kramer, E.J., 1996. Adhesion contact of cylindrical lens and a flat sheet. J. Appl. Phys. 80, 30–37.
Chen, S., Gao, H., 2006a. Non-slipping adhesive contact of an elastic cylinder on stretched substrates. Proc. R. Soc. London A 462, 211–228.
Chen, S., Gao, H., 2006b. Generalized Maugis–Dugdale model of an elastic cylinder in non-slipping adhesive contact with a stretched substrate. Int. J. Mater. Res. 97, 584–593.
Chen, S., Gao, H., 2007. Non-slipping adhesive contact between mismatched elastic cylinders. Int. J. Solids Struct. 44, 1939–1948.
Derjaguin, B.V., Muller, V.M., Toporov, Y.P., 1975. Effect of contact deformations on the adhesion of particles. J. Colloid Interface Sci. 53, 314–326.
Dugdale, D.S., 1960. Yielding of stress sheets containing slits. J. Mech. Phys. Solids 8, 100–104.
Greenwood, J.A., 1997. Adhesion of elastic spheres. Proc. R. Soc. London A 453, 1277–1297.
Greenwood, J.A., Johnson, K.L., 1998. An alternative to the Maugis model of adhesion between elastic spheres. J. Phys. D: Appl. Phys. 31, 3279–3290.
Haiat, G., Huy, M.C.P., Barthel, E., 2003. The adhesive contact of viscoelastic spheres. J. Mech. Phys. Solids 51, 69–99.
Hertz, H., 1882. On the contact of elastic solids. J. Reine Angew. Math. 92, 156–171.
Jin, F., Guo, X., Gao, H., 2013. Adhesive contact on power-law graded elastic solids: the JKR-DMT transition using a double-Hertz model. J. Mech. Phys. Solids 61, 2473–2492.
Johnson, K.L., 1985. Contact Mechanics. Cambridge University Press, Cambridge.
Johnson, K.L., Greenwood, J.A., 1997. An adhesion map for the contact of elastic spheres. J. Colloid Interface Sci. 192, 326–333.
Johnson, K.L., Greenwood, J.A., 2008. A Maugis analysis of adhesive line contact. J. Phys. D: Appl. Phys. 41, 155315-1–155315-6.
Johnson, K.L., Kendall, K., Roberts, A.D., 1971. Surface energy and the contact of elastic solids. Proc. R. Soc. London A 324, 301–313.
Kim, K.S., McMeeking, R.M., Johnson, K.L., 1998. Adhesion, slip, cohesive zones and energy fluxes for elastic spheres in contact. J. Mech. Phys. Solids 46, 243–266.
Liu, J., Notbohm, J.K., Carpick, R.W., Turner, K.T., 2010. Method for Characterizing Nanoscale Wear of Atomic Force Microscope Tips. ACS Nano 4, 3763–3772.
Maugis, D., 1992. Adhesion of spheres: The JKR-DMT transition using a Dugdale model. J. Colloid Interface Sci. 150, 243–269.
Morrow, C.A., Lovell, M.R., 2005. An extension to a cohesive zone solution for adhesive cylinders. J. Tribol. 127, 447–450.
Persson, B.N.J., 2002. Adhesion between and an elastic body and a randomly rough hard surface. Eur. Phys. J. E 8, 385–401.
Sari, O.T., Adams, G.G., Muftu, S., 2005. Nano-scale effects in the sliding and rolling of a cylinder on a substrate. J. Appl. Mech. 72, 633–640.
Sundaram, N., Farris, T.N., Chandrasekar, S., 2012. JKR adhesion in cylindrical contacts. J. Mech. Phys. Solids 60, 37–54.
Tabor, D., 1977. Surface forces and surface interactions. J. Colloid Interface Sci. 58, 2–13.
Zhang, W., Jin, F., Guo, X., Zhang, S., 2014. Adhesive contact on randomly rough surfaces based on the double-Hertz model. J. Appl. Mech. 81, 051008–1–7.